



The Physical Basis of Transparency in Biological Tissue: Ultrastructure and the Minimization of Light Scattering

SÖNKE JOHNSEN* AND EDITH A. WIDDER

*Marine Science Division, Harbor Branch Oceanographic Institution 5600 US 1 North, Ft. Pierce,
FL 34946, U.S.A.*

(Received 19 October 1998; Accepted in revised form on 1 April 1999)

In the open ocean, many animals are highly transparent, some achieving near invisibility. However, little is known about how this transparency is attained. The effects of cellular ultrastructure on tissue transparency were mathematically modeled. Given a specific constant volume or surface area of a higher refractive index material (e.g. protein, lipid, etc.), within a lower refractive index cytoplasm or other matrix, the model calculates the total amount of light scattered as a function of how the volume or surface area is subdivided. Given a constant volume, the scattering peaks strongly when the volume is divided into spheres of critical radii. The critical radii depend upon the refractive index of the material relative to its surroundings. Similarly, given a constant surface area, the scattering increases rapidly with sphere size until critical radii (approximating the critical radii for constant volume) are reached, after which the scattering is relatively constant. Under both constraints, refractive index is critical when the particles are small, but becomes progressively less important as particle size increases. When only forward scattering is considered, the results are essentially similar to those found for total scattering. When scattering at only larger angles is considered, the critical radii are independent of refractive index, and the scattered radiance depends critically on refractive index at all particle sizes. The effects of particle shape on scattering depend on the geometric constraint and particle size. Under constant volume constraints, small particles of any shape scatter light equally, but large spheres scatter less light than other larger shapes. Under constant surface area constraints, small spheres scatter more light than any small shape, but large particles of any shape scatter equally. The effects of crowding and the refractive index of the surrounding medium on these predictions are discussed.

© 1999 Academic Press

Introduction

Transparency is an important characteristic of oceanic zooplankton. A large and phylogenetically diverse number of these animals are transparent, some achieving almost complete invisibility (Greze, 1963, 1964; McFall-Ngai, 1990; Hammer, 1996; Johnsen & Widder, 1998), and it

is generally assumed that transparency is the primary method of camouflage for plankton in an otherwise optically featureless open-ocean environment (reviewed in Chapman, 1976a). However, despite the prevalence and presumed ecological importance of transparency in oceanic zooplankton, few attempts have been made to determine the physical basis for this characteristic (Chapman, 1976a, b). In contrast, there exists a large body of theoretical and experimental research on the physical basis of transparency of

* Author to whom correspondence should be addressed.
E-mail: sjohnsen@whoi.edu.

the mammalian cornea and lens (Trokkel, 1962; Benedek, 1971; Bettleheim, 1985; Tardieu & Delaye, 1988, Vaezy & Clark, 1994). These studies show that the biochemistry, microanatomy and ultrastructure of the lens and cornea are drastically modified for transparency (Goldman & Benedek, 1967; Philpson, 1973; Tardieu & Delaye, 1988). At present, it is not known how the tissues of any species of oceanic zooplankton are modified for transparency and how these modifications are compatible with life.

This study examines the effects of ultrastructure on transparency using mathematical models. The models calculate scattering by individual spherical particles and by groups of spherical particles under given total volume or surface area constraints and make predictions about certain aspects of the ultrastructure of transparent tissues. The models also consider the angular distribution of the scattered light, and make predictions related to the minimization of specific forms of scattering (e.g. backscatter, sidescatter). The effects of particle shape, crowding, and the refractive index of the surrounding medium on these predictions are also considered.

LIGHT ATTENUATION IN BIOLOGICAL TISSUE

An organism or tissue is transparent if it neither absorbs nor scatters light (Kerker, 1969). The majority of organic molecules do not absorb visible light (Tardieu & Delaye, 1988), and measurements of the wavelength dependence of light attenuation in over 30 species of transparent zooplankton show no evidence of absorption bands in the transparent regions (Johnsen & Widder, 1999). However, there are organic molecules that absorb light, and there are situations in which light absorption dominates light scattering for functional reasons, such as photoreception, protective pigments and warning coloration (Lythgoe, 1979). Here we exclusively consider light scattering.

It is important to make the distinction between transparency and invisibility. An invisible object is transparent, but a transparent object is not necessarily invisible. A transparent object with a high refractive index relative to the surrounding medium and a complex shape is visible due to light scattering at its edges (Hecht, 1998). For

example, a drop of water is transparent, but not invisible, due to the difference between the refractive index of water ($n = 1.33$) and air ($n = 1$). The same drop placed in water is both transparent and invisible, since the refractive index of the drop matches the refractive index of its surroundings. Here we primarily deal with transparency, rather than invisibility. A transparent object can be made less visible by matching its refractive index to that of its surroundings and by simplifying its external form (Kerker, 1969).

Scattering is caused by discontinuities in refractive index. A non-absorbing substance with a homogeneous refractive index is transparent. Biological tissue, however, has many refractive-index discontinuities. The discontinuities are due to the varying proportions and densities of lipids, proteins and other organic molecules. The refractive index of lipids is higher than that of cytoplasm (Meyer, 1979). Therefore, plasma membranes, lipid droplets and organelles with extensive folded membranes (e.g. mitochondria, Golgi apparatus and endoplasmic reticulum) have a higher refractive index than the surrounding cytoplasm. Organelles with dense protein concentrations, such as peroxisomes and lysosomes, also have a higher refractive index than the surrounding cytoplasm, as do nuclei, due to their high concentrations of nucleic acids.

PREVIOUS WORK ON LIGHT SCATTERING IN BIOLOGICAL TISSUE

Aside from work on the cornea and lens, no other research has been performed on transparent tissues. However, extensive studies of light scattering in biological tissue have been performed by optical oceanographers and medical researchers. Biological scattering research in optical oceanography has primarily concentrated on the scattering properties of phytoplankton and organic particulates, with the goal of linking the light-scattering characteristics of a body of water with the sizes and refractive indices of the embedded scatterers (Gordon & Brown, 1972; Meyer, 1979; Bricaud *et al.*, 1983; Quinby-Hunt & Hunt, 1988; Kitchen & Zaneveld, 1992). Non-ophthalmologic medical research into light scattering has been driven by the recent development of non-invasive optical methods for the diagnosis

and treatment of tissue (primarily skin) disorders (Mourant *et al.*, 1998). Researchers in this field are primarily interested in either correlating the scattering properties of tissue with various disorders or in determining the distance that (therapeutic) light will penetrate into a tissue (Wilson *et al.*, 1987; Beauvoit *et al.*, 1995, Beuthan *et al.*, 1996; Mourant *et al.*, 1998).

MIE SCATTERING

The amount of scattering is often given as a scattering cross-section, C_{sca} . The scattering cross-section of a particle is the cross-sectional area of a hypothetical opaque object whose shadow removes as much light as the particle removes from the original collimated light beam (Van de Hulst, 1957):

$$C_{sca} = A Q_{sca},$$

where A is the geometric cross-sectional area and Q_{sca} is the scattering efficiency of the particle. In general, the scattering efficiency of a particle depends on its size, shape, orientation and refractive index distribution. In the simplest case of scattering by a spherical object with a homogeneous refractive index,

$$A = \pi r^2,$$

and Q_{sca} depends on two ratios: (1) the radius of the sphere relative to the wavelength of the light beam in the surrounding medium, and (2) the refractive index of the sphere relative to the refractive index of the surrounding medium. Therefore,

$$C_{sca} = \pi r^2 Q_{sca}(r/\lambda_m, n_s/n_m),$$

where r is the radius of the sphere, λ_m is the wavelength of light in the surrounding medium, n_s is the refractive index of the sphere and n_m is the refractive index of the surrounding medium. The quotient of n_s and n_m is called the relative index and is usually denoted as m . Since

$$\lambda_m = \lambda_{vac}/n_m,$$

where λ_{vac} is the wavelength of light in a vacuum;

$$r/\lambda_m = rn_m/\lambda_{vac}.$$

The exact form of $Q_{sca}(rn_m/\lambda_{vac}, m)$ was first determined by Mie (1908). Mie also determined the radiance of scattered light, L , vs. angle, θ , relative to the direction of the original beam (θ equals zero for scattered light propagating in the same direction as the incident light). This function,

$$L = p(rn_m/\lambda_{vac}, m, \theta),$$

is generally referred to as the phase function (Van de Hulst, 1957). Both Q_{sca} and p are complex functions, and are seldom seen written in full form. Figure 1 shows the scattering cross-sections and phase functions of spheres of various sizes ($m = 1.1, n_m = 1, \lambda_m = 500$ nm). In general, the scattering cross-section increases with size, but the relationship between size and C_{sca} , and between size and the angular distribution of scattered light is neither simple nor intuitive.

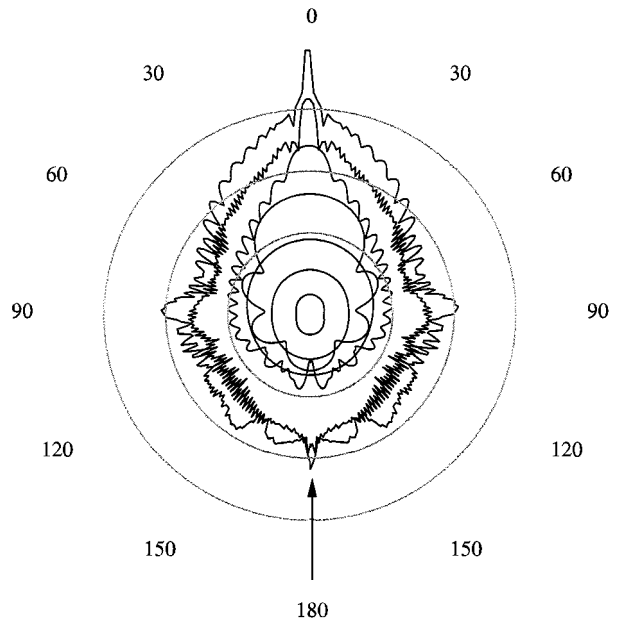


FIG. 1. The angular radiance distributions of scattered light by spheres of radii ranging from 5 nm to 20.5 μm ($m = 1.1, n_m = 1, \lambda_m = 500$ nm). The scattering distributions grow successively larger with sphere size. The data are normalized so that the forward scattered radiance of the smallest sphere equals 1. The scale is logarithmic; each circle indicates an increase by a factor of 1000. The seven sphere radii, with biological representatives, are $r = 5$ nm (globular proteins), $r = 20$ nm (ribosomes), $r = 80$ nm (centrosomes), $r = 320$ nm (lysosomes, peroxisomes), $r = 1.28$ μm (bacteria, small nuclei), $r = 5.12$ μm (small cells, large nuclei), $r = 20.5$ μm (large cells). The black arrow indicates the direction of the light beam.

TOTAL SCATTERING SUBJECT TO GEOMETRIC
CONSTRAINTS

A problem relevant to biological transparency is the minimization of light scattering caused by a given volume embedded within another volume. An example of this is fat storage within a cell. Lipids have a high refractive index relative to cytoplasm (Meyer, 1979), and therefore scatter light. If a cell contains a certain volume of lipid, is total scattering lower if the lipid is divided into many small spheres, or a small number of larger spheres? Note that the following arguments assume single scattering (that the scattering particles are separated by enough distance that scattered light from various scatterers does not destructively interfere). In addition, it is assumed that the spheres are randomly distributed. The Discussion section examines these assumptions and what results when they are violated.

Given a constant volume, V , divided into N spheres of equal radii r , the total scattering cross-section equals

$$C_{total} = NC_{sca} = N\pi r^2 Q_{sca}(rn_m/\lambda_{vac}, m).$$

Since,

$$V = 4N\pi r^3/3,$$

$$N = 3V/(4\pi r^3),$$

it follows that

$$\begin{aligned} C_{total} &= 3V/(4\pi r^3)\pi r^2 Q_{sca}(rn_m/\lambda_{vac}, m) \\ &= \mathbf{K}_v Q_{sca}(rn_m/\lambda_{vac}, m)/r, \end{aligned}$$

where $\mathbf{K}_v = 3V/4$ is a constant.

A second minimization problem relevant to biological transparency is the minimization of light scattering caused by a given total surface area. Surface area constraints are relevant in situations involving gas and fluid exchange and membrane transport. Given a constant surface area, S , divided into N spheres of equal radii r , the total scattering cross-section equals

$$C_{total} = NC_{sca} = N\pi r^2 Q_{sca}(rn_m/\lambda_{vac}, m).$$

Since

$$S = 4N\pi r^2,$$

$$N = S/(4\pi r^2),$$

it follows that

$$\begin{aligned} C_{total} &= S/(4\pi r^2)\pi r^2 Q_{sca}(rn_m/\lambda_{vac}, m) \\ &= \mathbf{K}_s Q_{sca}(rn_m/\lambda_{vac}, m). \end{aligned}$$

where $\mathbf{K}_s = S/4$ is a constant.

Materials and Methods

PARAMETERS

Scattering efficiency factors and phase functions were calculated using spheres with radii ranging from 1 nm to 100 μm . This range encompasses the sizes of many common intracellular and extracellular structures (Fig. 2). The refractive index of the surrounding medium was chosen to be that of cytoplasm ($n_m = 1.35$) (Charney & Bracket, 1961). Five relative refractive indices were used: 1.01, 1.05, 1.1, 1.2 and 1.5, resulting in absolute refractive indices of 1.36, 1.42, 1.49, 1.62 and 2.03. For comparison, the absolute refractive indices for various organic and non-organic substances are given in Table 1. The relative refractive indices used in the model were chosen to span the range of biological interest, except for the 1.5 value, which was used to provide an upper limit. Note that for relative refractive indices close to 1,

$$Q_{sca}(rn_m/\lambda_{vac}, 1 - x) \approx Q_{sca}(rn_m/\lambda_{vac}, 1 + x),$$

where x is the deviation of the relative refractive index from 1 (Van de Hulst, 1957). Therefore, the results of $m = 1.01, 1.05, 1.1,$ and 1.2 are roughly equivalent to the results for $m = 0.99, 0.95, 0.9$ and 0.8 .

As shown in Fig. 1, both the scattering cross-section and angular distribution of scattered light are a function of particle size. In particular, in the size range of most organelles, scatter is predominantly in the forward direction. This is particularly true when the relative refractive index, m , is close to 1. In some situations, scattering at

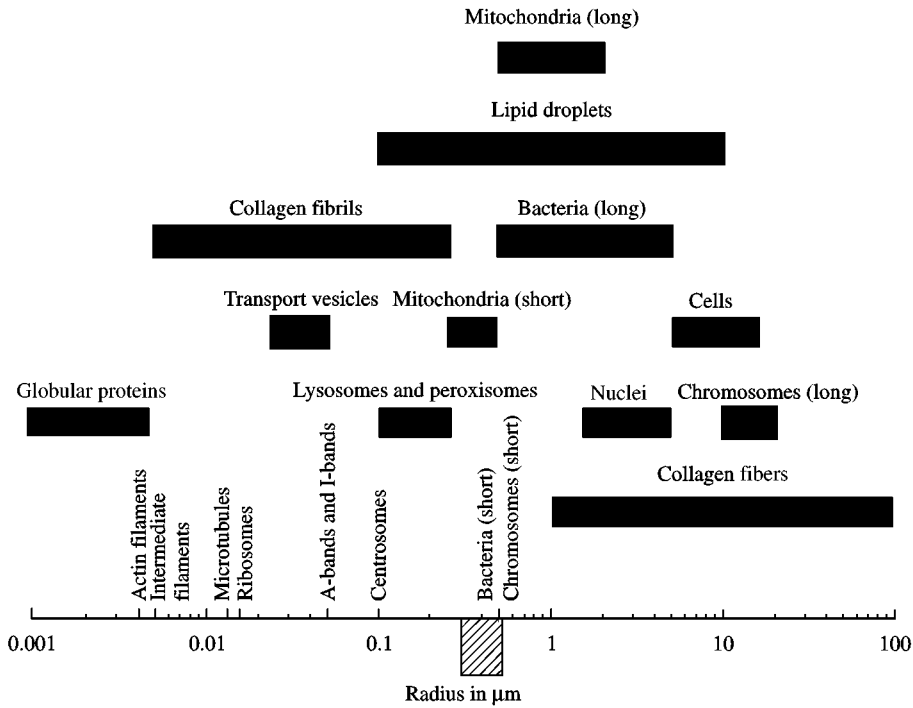


FIG. 2. The sizes (in radii) of various components of animal cells. For elliptical structures (e.g. bacteria), radii along the short axis and the long axis are given. For fibrous structures (e.g. microtubules) only the radii of the short axis are given. The exceptions to this are the values for the A-bands and I-bands of muscle, which are given as their lengths in longitudinal section. The hatched bar below the axis denotes the size range of visible wavelengths of light in water. Bacteria are included as cellular components because they are often ingested by animal cells. Values are taken from Alberts *et al.* (1994).

particular angles may be more important than total scattering. For example, an animal that needs to hide from viewers in a horizontal line of sight may minimize side scattering so that it is not revealed by downwelling light scattered towards the viewer. Similarly, an animal that needs to hide from a viewer above may minimize backward scattering. Therefore, the constant vol-

ume and constant surface area conditions were also modeled considering scattering in certain directions. The total scattering distribution was divided into four angular ranges, forward scattering ($1^\circ \leq \theta \leq 45^\circ$), forward side scattering ($46^\circ \leq \theta \leq 90^\circ$), backward side scattering ($91^\circ \leq \theta \leq 135^\circ$), and backward scattering ($136^\circ \leq \theta \leq 180^\circ$). The values for each of the four general scattering

TABLE 1
Absolute (n) refractive indices of various organic and inorganic components common to biological tissue

	Absolute refractive index	Reference
Calcite	1.57	CRC Handbook of Chemistry and Physics
Quartz	1.55	CRC Handbook of Chemistry and Physics
Cell membrane	1.46–1.60	Quinby-Hunt & Hunt (1988)
Cell membrane	1.46–1.54	Meyer (1979)
Collagen	1.55	Chapman (1976)
Cytoplasm	1.35	Charney & Brackett (1961)
Lipids	1.48	Beuthan <i>et al.</i> (1996)
Silica	1.39–1.42	Aas (1981)
Mitochondria	1.40	Beuthan <i>et al.</i> (1996)

directions are the average of the 45° values within each angular range.

The wavelength of light used in all the calculations was that of blue-green light (500 nm), close to the wavelength of maximum light penetration in clear ocean water (475 nm). This wavelength also simplifies mental calculations of scattering by other wavelengths. Since scattering is determined not by the absolute radius r , but by the relative radius r/λ_m , the scattering of a $1\ \mu\text{m}$ particle in 500 nm light is identical to the scattering of a $0.5\ \mu\text{m}$ particle in 250 nm light. Note that 500 nm is the wavelength of blue-green light in air. Since the refractive index of the surrounding medium was chosen to be that of cytoplasm ($n_m = 1.35$), the wavelength of blue-green light in this medium is $500/1.35 = 370\ \text{nm}$. The wavelength of the same light in seawater ($n = 1.33$) is 376 nm.

COMPUTATIONS

Scattering efficiency factors and phase functions for various sizes and relative refractive indices were calculated using Mietabtm (version 4.5, DAMIL Associates, Las Cruces, NM, U.S.A.). The Mietabtm software is based on numerical algorithms developed by Lentz (1976). The resulting values were analysed under constant volume and constant surface constraints using Excel (version 7.0, Microsoft Inc.).

Results

SINGLE PARTICLE

Figure 3 shows the scattering cross-section as a function of radius for individual spheres. The cross-section ranges over 21 orders of magnitude as particle size ranges over five orders of magnitude. For particles with radii less than approximately 70 nm, the scattering cross-section is proportional to the radius to the sixth power. For particles with radii greater than $10\ \mu\text{m}$, the scattering cross-section is proportional to the radius squared (i.e. proportional to the cross-sectional area of the sphere). In those particles with radii greater than 70 nm but less than $10\ \mu\text{m}$, the relationship between scattering cross-section and radius is complex and depends upon the relative refractive index.

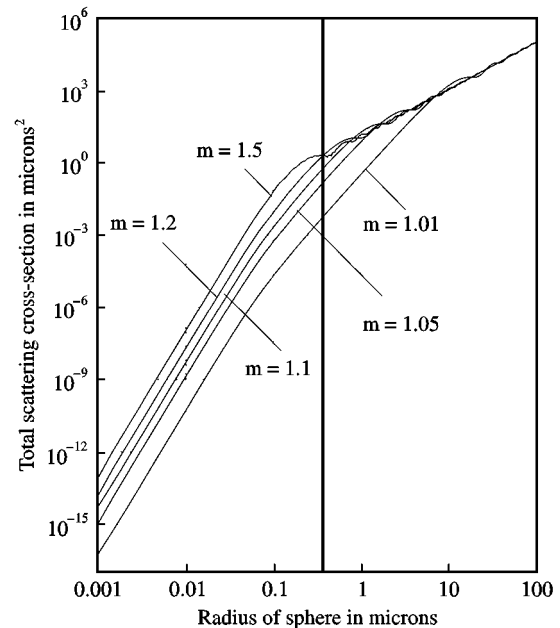


FIG. 3. The total scattering cross-section versus size for spheres with relative refractive indices (m) of 1.01, 1.05, 1.1, 1.2, and 1.5 in cytoplasm. The vertical line denotes the wavelength of blue-green light in cytoplasm ($n = 1.35$, $\lambda = 370\ \text{nm}$).

For particles with radii smaller than or roughly equal to the wavelength of light, scattering depends heavily on the relative refractive index, with particles with a refractive index of 1.2 scattering 230 times as much light as particles with a refractive index of 1.01. When the radius is greater than the wavelength of light, refractive index becomes progressively less important. When the radius is greater than $10\ \mu\text{m}$, the refractive index (given $m \geq 1.01$) has no effect on the scattering cross-section.

SCATTERING UNDER CONSTRAINTS OF CONSTANT SURFACE AREA AND CONSTANT VOLUME

Figure 4(a) shows the total scattering cross-section of a given constant surface area divided into spheres vs. the radii of those spheres. The total scattering cross-section for each refractive index increases rapidly with particle radius to a maximum value and then remains roughly constant. The critical radius, r_c , at which the maximum value is reached is inversely proportional to the refractive index, though the maximum total scattering cross-section is roughly independent of refractive index. The critical radii

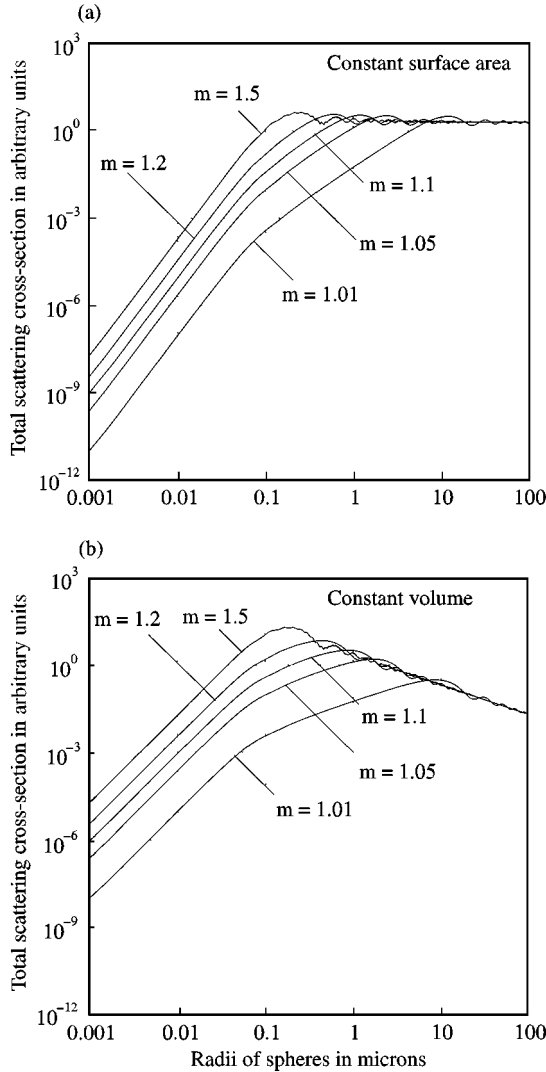


FIG. 4. (a) The total scattering cross-section for a given surface area divided into spheres of equal radii. (b) The total scattering cross-section for a given volume divided into spheres of equal radii.

are: $m = 1.5$, $r_c = 0.25 \mu\text{m}$; $m = 1.2$, $r_c = 0.60 \mu\text{m}$; $m = 1.1$, $r_c = 1.2 \mu\text{m}$; $m = 1.05$, $r_c = 2.4 \mu\text{m}$; $m = 1.01$, $r_c = 12 \mu\text{m}$.

Figure 4(b) shows the total scattering cross-section of a given constant volume divided into spheres vs. the radii of those spheres. The total scattering cross-section reaches a peak whose location and size depend upon the relative refractive index. The scattering cross-section falls off with spheres of larger or smaller radius, but more quickly with spheres of smaller radius. In neither direction though, does the total scattering cross-section fall off as quickly with radius as is seen

in the constant surface area case. The critical radii where the peak total scattering occurs are: $m = 1.5$, $r_c = 0.21 \mu\text{m}$; $m = 1.2$, $r_c = 0.44 \mu\text{m}$; $m = 1.1$, $r_c = 0.94 \mu\text{m}$; $m = 1.05$, $r_c = 1.7 \mu\text{m}$; $m = 1.01$, $r_c = 9.0 \mu\text{m}$.

Under both constant surface area and constant volume constraints, as the radii of the spheres increases beyond the wavelength of light, refractive index becomes progressively less important. For radii greater than $10 \mu\text{m}$, relative refractive index (given $m \geq 1.01$) has no effect on the total scattering cross-section.

SCATTERING AT DIFFERENT ANGLES

Figures 5 and 6 show the total scattered radiance of a group of spherical particles with a given total surface area or volume averaged over the following four directions: forward scattering ($1^\circ \leq \theta \leq 45^\circ$) [Figs 5(a) and 6(a)], forward-side scattering ($46^\circ \leq \theta \leq 90^\circ$) [Figs 5(b) and 6(b)], backward side scattering ($91^\circ \leq \theta \leq 135^\circ$) [Figs 5(c) and 6(c)] and backward scattering ($136^\circ \leq \theta \leq 180^\circ$) [Figs 5(d) and 6(d)]. In the case of forward scattering, the relationships between particle size and scattered radiance are similar to those found for total scattering. The critical radii are found at roughly the same locations as in the total scattering case. Also, as in the case of total scattering, the forward-scattered radiance does not depend heavily on relative refractive index when the radii of the particles are greater than $10 \mu\text{m}$.

For the cases of forward-side, backward-side, and backward scattering, the relationships between scattered radiance and particle radii are different from the total scattering case. Under both constant surface area and constant volume constraints, the critical radii are independent of the refractive index (for forward-side scatter $r_c \approx 0.2 \mu\text{m}$, for backward-side and backward scatter $r_c \approx 0.07 \mu\text{m}$). The constant value reached, however, depends strongly on the refractive index. The dependence on the refractive index grows larger as the scattering angle increases. In all four directions, particularly in backward scattering, the relationship between the radii of the spheres and the scattered radiance develops considerable oscillations at super-critical radii.

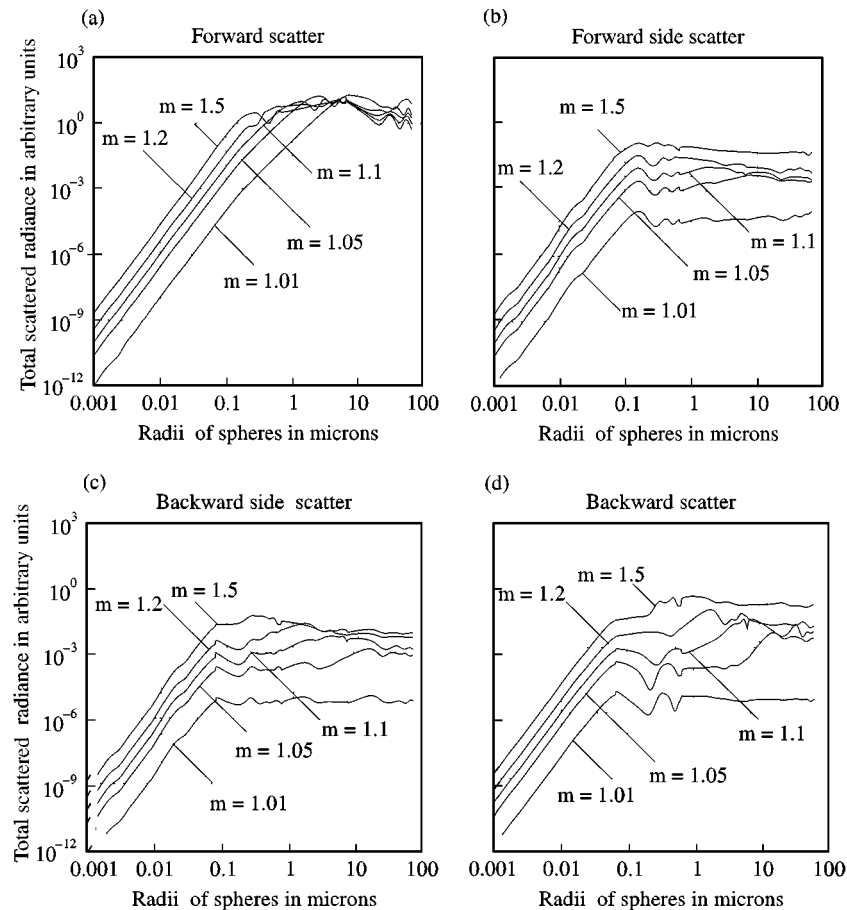


FIG. 5. The total scattered radiance in various directions for a given surface area divided into spheres of equal radii. (a) Forward scattered radiance, (b) forward-side scattered radiance, (c) backward-side scattered radiance, (d) backward scattered radiance.

Discussion

THEORIES OF TISSUE TRANSPARENCY

There are several methods of achieving transparency. The two methods that are simplest in conception, if not execution, are: (1) extreme flattening perpendicular to the visual axis, and (2) having a homogeneous refractive index. Flattening perpendicular to the visual axis is successful because light attenuation (due to scattering or absorption) is exponentially proportional to path length. Therefore, even tissue that scatters a large amount of light per unit length can be quite transparent if the path length is made short enough (even metals are transparent in thin layers). For example, eel leptocephalus larvae and certain pelagic crustaceans (e.g. the decapod shrimp *Lucifer*, stomatopod larvae) employ this

method of achieving transparency. This method has the added advantage of also making the animal difficult to detect end-on.

Any tissue with a homogeneous refractive index will also be transparent. In the strictest sense, this requires that either the tissue is made up of only one component, or that it is made up of different components that all have the same refractive index. Given that refractive indices of organic compounds are quite variable and often correlated with molecular weight, this is hard to achieve. It does, however, raise the interesting possibility that certain transparent animals contain "clearing" agents; inert substances with refractive indices close to that of protein that raise the refractive index of the ground substance and thus reduce the relative refractive indices and, therefore, scattering. While this increases

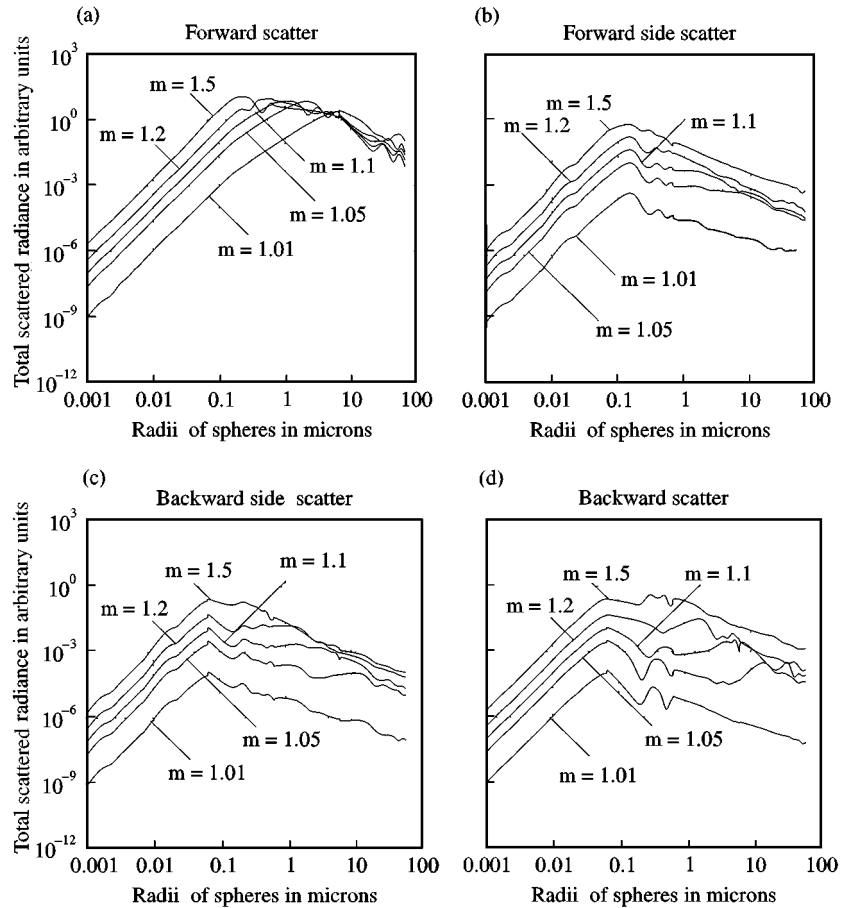


FIG. 6. The total scattered radiance in various directions for a given volume divided into spheres of equal radii. (a) Forward scattered radiance, (b) forward-side scattered radiance, (c) backward-side scattered radiance, (d) backward scattered radiance.

the animal's transparency, it may decrease its invisibility, since the entire animal will be a high-refractive-index object within a low-refractive-index medium (the surrounding water).

While a completely homogeneous refractive index is sufficient for transparency, it is not always necessary. A tissue can have components with many different refractive indices, so long as the average refractive index is constant over distances equal to half the wavelength of light or more (Benedek, 1971). In other words, scattering and light attenuation are low if the spatial distribution of refractive index has no Fourier components with wavelengths greater than one-half the wavelength of light. This low scattering is due to extensive destructive interference of the scattered light from the various scatterers. What is observed instead is a slower speed of light through the material. In short, scattering (in the presence

of heavy destructive interference) is the source of refractive index. For example, in glass each of the various molecules scatter light, but due to destructive interference no scattered light is observed and the beam is not attenuated. This theory has been invoked to explain the transparency of the mammalian cornea and lens (Benedek, 1971; Tardieu & Delaye, 1988; Vaezy & Clark, 1994). In both tissues, a substance with a high refractive index (collagen fibers in the cornea and crystalline proteins in the lens) is embedded within a substance with a low refractive index. The high refractive index substance is packed so densely the steric and other repulsive interactions force a local ordering of the scatterers (Tardieu & Delaye, 1988). The ordering exists only over distances on the order of several diameters of the scatterers, but is sufficient to drastically reduce scattering. In the case of N identical scatterers,

the total scattering cross-section, C_{total} , is given by

$$C_{total} = NC_{sca}S(\phi),$$

where C_{sca} is the scattering cross-section of an individual scatterer, ϕ is the volume concentration of the scatterers ($V_{scatterers}/V_{total}$) and $S(\phi)$ is the structure factor. The structure factor gives the amount of reduction in total scattering due to destructive interference caused by local ordering. In general, $S(\phi)$ is complex or unknown (see Benedek, 1971), but in the simpler case of small scatterers ($r \leq 70$ nm) it is

$$S(\phi) = (1 - \phi)^4 / (1 + 4\phi + 4\phi^2 - 4\phi^3 + \phi^4)$$

(Delaye & Tardieu, 1983).

Figure 7(a) shows the structure factor vs. the volume concentration of the scatterers. A concentration of scatterers of 30% reduces the total scattering to 10% of the value calculated under the assumption of no destructive interference of scattered light. A concentration of 60% reduces the scattering to less than 1% of the value calculated assuming no destructive interference. Figure 7(b) shows the total scattering cross-section of a number of small particles vs. their volume concentration. As the volume concentration increases, there are more scatterers, but also more destructive interference. The maximum total scattering occurs at 13% concentration with total scattering actually decreasing as the number of scatterers increases beyond this concentration [see Benedek (1971) and Tardieu & Delaye (1988) for further details]. This theory has been experimentally confirmed using solutions of lens proteins (Bettleheim & Siew, 1983). The solution becomes cloudier with increasing concentration, until a volume concentration of approximately 13%, after which it becomes clearer.

It is important to note, however, that the above theory does not imply that objects with dimensions less than half a wavelength do not scatter light. A thin flat sheet (perpendicular to the light beam) may have a thickness less than the wavelength of light, but it has Fourier components of many wavelengths, some of which are greater than the wavelength of light (Hecht, 1998).

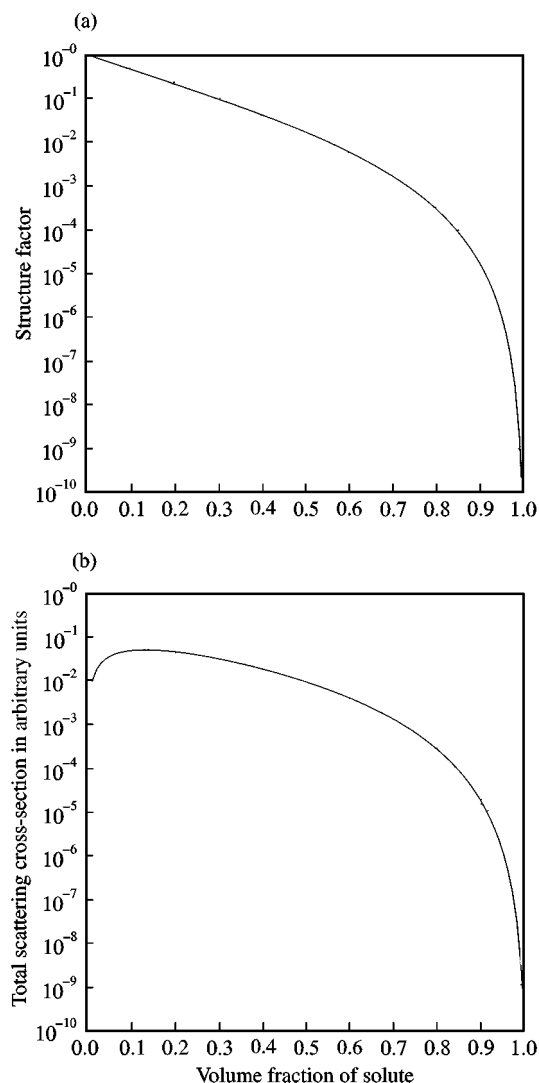


FIG. 7. (a) The structure factor for small identical scatterers vs. their volume fraction. (b) The total scattering cross-section of a collection of small scatterers vs. their volume fraction.

Therefore it still scatters light. It is for this reason that a microscope can detect an object smaller than the resolution limit if it is situated on an empty background.

OPTIMIZATION OF TRANSPARENCY GIVEN A CONSTANT SURFACE AREA OR VOLUME

The above theory is very likely applicable to explaining the transparency of certain extracellular structures in transparent zooplankton (e.g. mesoglea), but it cannot adequately help to understand transparency in intracellular components. Reduction of scattering by destructive

interference relies on dense packing of similar objects. In the two cases where this theory has been successfully applied, the tissues are highly simplified. The mammalian lens, in particular, has been drastically modified for transparency (Goldman & Benedek, 1967; Philipson, 1973; Tardieu & Delaye, 1988). Most of the lens cells lack nuclei, mitochondria and other organelles, and, in fact, are little more than containers for dense concentrations of few different proteins. The cells rely entirely on the surrounding cells for metabolic support and maintenance. These modifications are obviously incompatible with life when employed throughout an entire organism.

This study examines the optimization of transparency in tissues that cannot be simplified in the ways seen in the cornea and lens. The models, while simplified, make several interesting and non-intuitive predictions. The first set of predictions involve the consideration of total scattering in all directions. When a given volume of a substance must be present within a tissue or cell, the volume will be apportioned into particles with radii greater or smaller than a certain critical radius. The critical radius will depend on the refractive index of the particle; for blue-green light in cytoplasm, the critical radius is approximately given by

$$r_c \approx 0.1/(m - 1).$$

When a given surface area of a substance must be present, the surface area will be apportioned into particles with radii smaller than a critical radius (which approximates the critical radius under constant volume constraints). Increasing particle radius beyond the critical radius does not appreciably decrease total scattering. In both situations, particles with radii less than 10 μm will have low relative refractive indices, though this tendency will be more marked in smaller particles. Particles with radii larger than 10 μm will not tend to have low refractive indices, unless the index can be brought below 1.01. In cases where the refractive index can only be varied over a certain range (e.g. altering the refractive index of collagen by varying hydration), particles beyond a certain size will not tend to have low refractive indices.

In situations where only forward scattering is important, the predictions are essentially similar to the predictions for total scattering. In situations where side-scatter and especially backscatter are important, the predictions are different. Under constant volume constraints, particles will have radii greater or less than a certain critical radius. This radius however, does not depend on the refractive index of the particles. For blue-green light, the critical radius is approximately 0.2 μm for forward-side scatter and 0.07 μm for scattering at higher angles. Under constant surface area constraints, particles will have radii smaller than the critical radius. Under either constraint, particles will have low relative refractive indices at all particle sizes.

These predictions are all, of course, subject to additional constraints unrelated to transparency. However, given the strong dependence of scattering on size, especially under constant surface area constraints, any component that can change its size at all can substantially reduce total scattering.

EFFECTS OF PARTICLE SHAPE ON SCATTERING

While certain cellular components are almost perfectly spherical (e.g. lipid vesicles), many are not. How this effects the predictions of this study depends on the size of the particles. For particles whose dimensions are all less than approximately 70 nm and whose relative refractive indices less than or equal to 1.2, particle shape and orientation have no effect on Q_{sca} . Large proteins, protein complexes, transport vesicles and ribosomes all fall within this range. For particles with the above characteristics (and *only* for these particles),

$$C_{sca} = k^4 V^2 (m^2 - 1)^2 / (6\pi),$$

where V is the volume of the particle and $k = 2\pi/\lambda$ (van de Hulst, 1957). Therefore,

$$C_{total} = N C_{sca} = N k^4 V^2 (m^2 - 1)^2 / (6\pi).$$

Given a constant volume, V , divided into N small particles,

$$V = NV$$

and

$$C_{total} = \mathbf{V}/V k^4 V^2 (m^2 - 1)^2 / (6\pi) = \mathbf{K}_v V (m^2 - 1)^2,$$

where $\mathbf{K}_v = k^4 \mathbf{V} / (6\pi)$ is a constant. Therefore, in the constant volume case, C_{total} is linearly proportional to the volume of the individual particles. Given a constant surface area, \mathbf{S} , divided into N particles (given the same restrictions on size and refractive index found in the above constant volume case),

$$\mathbf{S} = NS$$

and

$$\begin{aligned} C_{total} &= \mathbf{S}/S k^4 V^2 (m^2 - 1)^2 / (6\pi) \\ &= \mathbf{K}_v V^2 (m^2 - 1)^2 / S, \end{aligned}$$

where $\mathbf{K}_v = k^4 \mathbf{S} / (6\pi)$ is a constant. Therefore, in the constant surface area case, C_{total} is linearly proportional to the volume of the individual particles multiplied by the quotient of volume and surface area, V/S . Since a sphere has the greatest volume per surface area, the total scattering in the constant surface area case is higher for spheres than for any shape. The two predictions resulting from the above analysis of scattering by small particles of arbitrary shape are: (1) under constant volume constraints, there will be no selection for particular particle shapes, and (2) under constant surface area constraints, there will be selection for non-spherical particles.

For large particles (radii several times the critical radius) of arbitrary shape with biologically realistic refractive indices, $Q_{sca} \approx 2$ (Van de Hulst, 1957). Large vacuoles, mitochondria, and nuclei all fall into this range. This approximation is not exact. For supercritical spheres with a relative refractive index of 1.2, $1.7 < Q_{sca} < 2.7$ and approximates 2 to within 10% when spheres have radii greater than approximately 4.5 μm . For spheres with a lower relative refractive index, the range of Q_{sca} is less [see Fig. 4(a)]. C_{total} for a constant volume, \mathbf{V} , divided into N large particles is

$$C_{total} = N C_{sca} \approx 2NA,$$

where A is the cross-section of one particle. Now,

$$N = \mathbf{V}/V,$$

where V is the volume of one particle. Therefore,

$$C_{total} \approx 2A\mathbf{V}/V = \mathbf{K}_v A/V,$$

where $\mathbf{K}_v = 2\mathbf{V}$ is a constant. By similar reasoning, given a constant surface area, \mathbf{S} ,

$$C_{total} \approx 2A\mathbf{S}/S = \mathbf{K}_s A/S,$$

where S is the surface area of one particle, and $\mathbf{K}_s = 2\mathbf{S}$ is a constant. Therefore, in the constant volume and constant surface area cases for large particles, the total scattering depends on A/V and A/S respectively. Since the orientation of the beam of light relative to the particle is likely to be random, we use the average cross-section over all orientations, A_{avg} . Remarkably, for any convex solid A_{avg} is always one-fourth the total surface area (see the appendix). Therefore, A_{avg}/S is independent of shape and A_{avg}/V equals $S/(4V)$. For example, for a cylinder with radius r and length l ,

$$A_{avg}/S = 1/4$$

and

$$\begin{aligned} A_{avg}/V &= S/(4V) = (2\pi r^2 + 2\pi r l)/(4\pi r^2 l) \\ &= (r + l)/(2rl) = \frac{1}{2}(1/l + 1/r). \end{aligned}$$

Figure 8 shows the total scattering cross-section for a collection of large cylinders of constant volume versus the ratio of radius of length (i.e. aspect ratio). The minimum scattering occurs when the diameter equals the length. Of all shapes, the optimum is the sphere since it has the minimum surface area. The two predictions resulting from the analysis of scattering by large particles of arbitrary shape are: (1) under constant volume constraints, there will be selection for spherical shapes, and (2) under constant surface area constraints, there will be no selection for particular shapes. Note that these predictions are nearly opposite from those obtained for small particles.

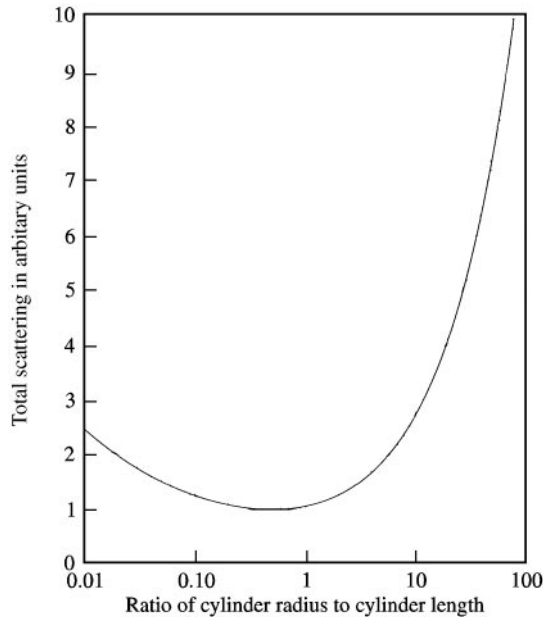


FIG. 8. The total scattering cross-section vs. shape for a collection of large cylinders of constant volume. Shape is given as the ratio between the radius of the cylinder and the length.

The above analyses do not consider particles with radii greater than 70 nm but less than several times the critical radius. In this range, the relationship between shape and scattering is highly complicated and few generalizations can be made (Kerker, 1969). Using finite element methods, Thiele (1998) showed that, for titanium oxide ($n = 2.74$) under constant volume constraints, spheres with critical radii scattered approximately the same amount of light as rhomboidal crystals with the same volume.

The effect of particle shape on scattering is considerably less than the effects of particle size and refractive index. For both small and large particles, the effects of fairly drastic changes in shape are moderate compared to the effects of similar changes in size or refractive index (compare Figs 4 and 8).

EFFECTS OF CROWDING

As mentioned above, the total scattering of a group of particles depends on the crowding of the particles. This is due to destructive interference between scattered light from the various scatterers. The exact relationship between crowding and reduction of scattering for particles with

radii greater than approximately half the wavelength of light is at present impossible to calculate for any biologically realistic situation. Computer simulations involving scattering of groups of 10–100 particles (Thiele, 1998) have shown that groups of smaller particles behave approximately like larger particles, with the associated change in scattering per volume. Particles with biological relative refractive indices ($m \leq 1.2$) can be considered part of a group when they are within one wavelength of another particle (McNeil, pers. comm.). The crowding effect can reduce scattering in cellular tissue. For example, if a particular cellular component (e.g. lysosome) has a radius near the critical radius for maximum scattering per volume, and its size cannot be altered, it can be grouped with other components to lower the scattering per volume.

The crowding effect is also important in the case of fibers. Many intra- and extracellular fibers have radii far less than the wavelength of light, but lengths far greater. Often they are bundled into larger fibers, which affects total scattering. For long, thin cylinders, Q_{sca} depends on orientation in a complicated way, but in general is proportional to the cube of the radius of the fiber [see Van de Hulst (1957) for individual formulae]. Therefore,

$$C_{total} = NC_{sca} = NAQ_{sca} \propto NIR^4,$$

where N is the number of fiber bundles, and R and l are the radius and length of each bundle. Given a constant volume V of fibers,

$$V = N\pi R^2 l.$$

Therefore,

$$N = V/(\pi R^2 l) \quad \text{and} \quad C_{total} \propto R^2.$$

Since the total scattering of a constant volume of fibers is proportional to square of the radii of the bundles, the prediction for transparent tissues is that fibers will not be bundled. Note that this relationship is only valid for fiber bundles with $R \leq 70$ nm. For large R , the discussion of average cross-sectional areas applies. For intermediate R , the predictions are more complicated and are not discussed here.

EFFECTS OF REFRACTIVE INDEX
OF SURROUNDING MEDIUM

As mentioned in the introduction, Q_{sca} does not depend on the absolute size of a particle, but on its size relative to the wavelength of light. Since the wavelength depends on the medium's refractive index, n_m , we find that Q_{sca} depends on rn_m/λ_{vac} . Therefore, changing the refractive index of the surrounding medium alters the scattering curves, even if the relative refractive indices remain constant. Increasing n_m shifts the curves in Figs 3–8 to the left. Under constant surface area constraints, this either increases total scattering or leaves it unaffected. Under constant volume constraints, this increases total scattering for particles with sub-critical radii, but decreases total scattering for particles with super-critical radii. Decreasing n_m has the opposite effects. Of course, if n_s does not also change, then changing n_m will change the relative refractive index of the scatterers (since $m = n_s/n_m$). These two effects either work in concert or opposition depending on the sizes of the particles and the particular geometric constraint.

SUMMARY AND APPLICATION OF PREDICTIONS

This study's predictions for the ultrastructure of transparent tissue are summarized in Table 2. The parameters affecting light scattering are listed in descending order of importance. The predictions for transparent tissues under the constant surface area and constant volume constraints are then given for each parameter in the most general form possible. One can see that the predictions depend on many factors in complex and often surprising ways.

A brief example may be useful in clarifying the application of these predictions to a biological situation. Consider a "typical" animal cell that scatters a minimum amount of blue-green light in any direction. Table 3 lists the predictions for various cell components. For each component, a range of size and relative refractive index is given. All the components are considered to be primarily bound by constant volume constraints, with the exception of mitochondria. Since mitochondrial functioning depends heavily on the amount of membrane, it is considered to be bound by constant surface area constraints. The

absolute refractive index of the cytoplasm is assumed to be 1.35. The relative refractive indices are highly approximate and based on values of 1.2 for protein, 1.1 for lipid and 0.99 for saline. In cases where are given prediction cannot be applied (e.g. dividing a nucleus into smaller nuclei, changing the shape of a microtubule), no prediction is made. All predictions assume that the size and refractive index of a given component must remain within the range given.

It is important to remember that these predictions assume that a certain amount of each material must be present within the cell. Since scattering cross-section always increases with particle size, transparency can, of course, be increased by reducing the total amount of material within the cell. However, as mentioned above, a functioning cell must have a minimum amount of certain organelles and other intracellular material. The above predictions assume that the cell already has a functional minimum of intracellular material.

USE OF ATTENUATION SPECTRA TO EXAMINE
INTERNAL STRUCTURE

Since Q_{sca} does not depend on the absolute value of the particle radius, but on the particle radius relative to the wavelength of light, in theory one can determine particle size from the spectrum of light scattered from a particle. In general, the scattering cross-section is proportional to wavelength, i.e.

$$C_{sca} \propto \lambda^k,$$

For small particles, $k = -4$, for particles with radii near the wavelength of light, $-4 < k < 0.2$ and for large particles, $k = 0$ [see Fig. 4(a), which is essentially a graph of Q_{sca} vs. radius]. In practice, however, determining the size of particles from the scattering spectrum is complicated by even slight absorption, crowding effects and by the fact that the particles in a given realistic situation are seldom all the same size. See Kerker (1969) for a detailed treatment of the possibilities and limitations of determining particle size from scattering spectra.

Johnsen & Widder (1998) measured the attenuation spectra of various transparent tissues and

TABLE 2

Summary of the ultrastructural predictions for transparent tissues. The left column lists the various parameters in order of their importance to tissue transparency. The two remaining columns list the predictions for the given parameter under constant surface area and constant volume constraints. As mentioned in the text, forward scattering is defined as scattering at angles less than 45° . Particles are considered small if their radii are small relative to the wavelength of light and large if their radii are several times greater than the critical radius given in the table. Particles are considered clustered if they are within a wavelength of light of each other

	Constant surface area constraint	Constant volume constraint
Size of particles into which substance is subdivided in cases of total or forward scattering	<p>Particles will have radii less than a certain critical radius</p> <p>Critical radius depends on the relative refractive index and is given by $r_c \approx 0.1/(m - 1)$</p>	<p>Particles will have radii either greater or less than a certain critical radius</p> <p>Critical radius is approximately equal to critical radius under the constant surface area constraint</p>
Size of particles into which substance is subdivided in cases of scattering at larger angles	<p>Particles will have radii less than a certain critical radius</p> <p>Critical radius is independent of the relative refractive index and is given by $r_c \approx 0.2 \mu\text{m}$ for forward-side scatter $r_c \approx 0.07 \mu\text{m}$ for scattering at higher angles</p>	<p>Particles will have radii either greater or less than a certain critical radius</p> <p>Critical radius is approximately equal to critical radius under the constant surface area constraint</p>
Clustering or dispersion of particles	<p>Small particles will be dispersed</p> <p>Large particles will have no special distribution</p>	<p>Small particles will be dispersed</p> <p>Large particles will be clustered</p>
Relative refractive index of particles in cases of total or forward scattering	<p>Small particles will have low relative refractive indices</p> <p>Large particles will have arbitrary refractive indices</p>	<p>Small particles will have low relative refractive indices</p> <p>Large particles will have arbitrary refractive indices</p>
Relative refractive index of particles in cases of scattering at larger angles	All particles will have low relative refractive indices	All particles will have low relative refractive indices
Shape for small particles	Particles will not be spherical	Particle shape will be arbitrary
Shape for medium-sized particles	Predictions are highly case-specific	Predictions are highly case-specific
Shape for large particles	Particle shape will be arbitrary	Particles will be spherical
Refractive index of medium (assuming relative refractive index of particle remains constant)	Refractive index of medium will be low	Predictions are highly case-specific

fit the curves to the above equation. For the most transparent tissues, k ranged from -2 to -1 . For moderately transparent tissues, k ranged from -0.78 to -0.11 . For the nearly opaque tissues, k approximated zero. This suggests that the attenuation of light in the highly and moder-

ately transparent tissues sampled is mostly due to light scattering by medium-sized particles and that the attenuation in the nearly opaque tissues is mostly due to scattering by large particles. However, due to the complications mentioned above, further work is needed to confirm this.

TABLE 3

Predictions for a typical cell that scatters a minimum amount of light. The predictions cover the shape, distribution (many and small, few and large) and refractive index of the cellular components

	Constraint	Size	m	Predictions
Actin filaments Intermediate filaments Microtubules	Volume	4 nm 5 nm 12 nm	1.15–1.2	Shape: not applicable Distribution: dispersed Refractive index: low
Ribosomes	Volume	15 nm	1.15–1.2	Shape: arbitrary Distribution: dispersed Refractive index: low
Transport vesicles	Volume	15–50 nm	1.1–1.2	Shape: arbitrary Distribution: many, small, and dispersed Refractive index: low
Lysosomes Peroxisomes	Volume	0.1–0.25 μm	1.1–1.2	Shape: difficult to predict Distribution: many, small, and dispersed Refractive index: low
Lipid droplets	Volume	0.1–0.10 μm	1.1–1.2	Shape: arbitrary (if droplets are large, then spherical) Distribution: many, small, and dispersed Refractive index: low (if droplets are large, then arbitrary within range)
Mitochondria	Surface area	0.25–10 μm	1.05–1.1	Shape: difficult to predict Distribution: many, small, and dispersed Refractive index: low (if mitochondria are large, then arbitrary within range)
Nucleus	Volume	1.5–5 μm	1.05–1.1	Shape: spherical Distribution: not applicable Refractive index: arbitrary within range
Large vacuole	Volume	5–15 μm	0.99–1.2	Shape: spherical Distribution: few, large, and clustered refractive index: arbitrary unless it can be brought to 1.01 or less

THE MAXIMIZATION OF SCATTERING

While its primary purpose is to understand the minimization of scattering, the theory described in this paper can also be applied to understanding the inverse problem; the maximization of scattering. Maximization of scattering is important to animals with structural pigments, iridophores or reflective surfaces, since all these cases are examples of strong scattering by high refractive index materials within a low refractive index matrix (Land, 1978; Prum *et al.*, 1999). As a final note, there are animals that deliberately change their transparency. When disturbed, the

highly transparent siphonophore *Hippopodius hippopus* becomes opaque within a matter of seconds, due to the formation of granules within its tissue (Mackie, 1996). This increase in scattering can be understood within the context of the constant volume case shown in Fig. 4(b). Since the opacity occurs too quickly for the particles to be created *de novo*, the increase in scattering is due to the grouping of a given volume into larger particles. Since the particles are smaller than the critical radius (for dense protein in a cytoplasmic base, r_c is approximately equal to 0.5 μm in blue–green light), this increases scattering dramatically.

We thank Dr Laurie McNeil for considerable instruction in the subtler aspects of the physics of light scattering, and for pointing us to relevant literature in surprising places. We also thank Dr Christopher Herald for the geometric proof found in the appendix, and Drs Tamara Frank, William Kier and Laurie McNeil for a critical reading of the manuscript. This work was funded by a Harbor Branch Institution Postdoctoral Fellowship to SJ. This is Harbor Branch Contribution No. 1283.

REFERENCES

- AAS, E. (1981). The refractive index of phytoplankton, *Univ. Oslo Rep. Ser.* 46.
- ALBERTS, B., BRAY, D., LEWIS, J., RAFF, M., ROBERTS, K. & WATSON, J. D. (1994). *Molecular Biology of the Cell*, 3rd edn. New York: Garland Publishing Inc.
- BEAUVOIT, B., EVANS, S. M., JENKINS, T. W., MILLER, E. E. & CHANCE, B. (1995). Correlation between the light scattering and the mitochondrial content of normal tissues and transplantable rodent tumors. *Anal. Biochem.* **226**, 167–174.
- BENEDEK, G. B. (1971). Theory of the transparency of the eye. *Appl. Opt.* **10**, 459–473.
- BETTLEHEIM, F. A. (1985). Physical basis of transparency. In: *The Ocular Lens: Structure, Function, and Pathology* (MAISEL, H., ed.), pp. 265–300. New York: Dekker.
- BETTLEHEIM, F. A. & SIEW, E. L. (1983). Effect of change in concentration upon lens turbidity as predicted by the random fluctuation theory. *Biophys. J.* **41**, 29–33.
- BEUTHAN, J., MINET, O., HELFMANN, J., HERRIG, M. & MUELLER, G. (1996). That spatial variation of the refractive index in biological cells. *Phys. Med. Biol.* **41**, 369–382.
- BRICAUD, A., MOREL, A. & PRIEUR, L. (1983). Optical efficiency factors of some phytoplankters. *Limnol. Oceanogr.* **18**, 816–832.
- CHAPMAN, G. (1976a). Reflections on transparency. In: *Coelenterate Ecology and Behavior* (Mackie, G. O., ed.), pp. 491–498. New York: Plenum Press.
- CHAPMAN, G. (1976b). Transparency in organisms. *Experientia* **15**, 123–125.
- CHARNEY, E. & BRACKETT, F. S. (1961). The spectral dependence of scattering from a spherical alga cell and its implication for the state of organization of the light accepting pigments. *Arch. Biochem. Biophys.* **92**, 1–12.
- DELAYE, M. & TARDIEU, A. (1983). Short-range order of crystallin proteins accounts for eye lens transparency. *Nature* **302**, 415–417.
- GOLDMAN, J. N. & BENEDEK, G. B. (1967). The relationship between the morphology and transparency in the non-swelling corneal stroma of the shark. *Invest. Ophthalmol.* **6**, 574–600.
- GORDON, H. R. & BROWN, O. B. (1972). A theoretical model of light scattering by Sargasso Sea particulates. *Limnol. Oceanogr.* **17**, 826–832.
- GREZE, V. N. (1964). The determination of transparency among planktonic organisms and its protective significance. *Dokl. Akad. Nauk. S.S.S.R.* **151**, 435–438.
- GREZE, V. N. (1964). The transparency of planktonic organisms in the equatorial part of the Atlantic Ocean. *Okeanologiya* **4**, 125–127.
- HAMNER, W. M. (1996). Predation, cover, and convergent evolution in epipelagic oceans. In: *Zooplankton: Sensory Ecology and Physiology* (LENZ, P. H., HARTLINE, D. K., PURCELL, J. E. & MACMILLAN, D. L., eds), pp. 17–37. Amsterdam: Overseas Publishers Association.
- HECHT, E. (1998). *Optics*. New York: Addison-Wesley Longman Inc.
- JOHNSEN, S. & WIDDER, E. A. (1998). The transparency and visibility of gelatinous zooplankton from the north west Atlantic and Gulf of Mexico. *Biol. Bull.* **195**, 337–348.
- KERKER, M. (1969). *The Scattering of Light and Other Electromagnetic Radiation*. New York: Academic Press.
- KITCHEN, J. C. & ZANEVELD, J. R. V. (1992). A 3-layered sphere model of the optical properties phytoplankton. *Limnol. Oceanogr.* **37**, 1680–1690.
- LAND, M. F. (1978). Animal eyes with mirror optics. *Sci. Am.* **239**, 126–134.
- LENTZ, W. J. (1976). Generating Bessel functions in Mie scattering calculations using continued fractions. *Appl. Opt.* **15**, 668.
- LYTHGOE, J. N. (1979). *The Ecology of Vision*. Oxford: Clarendon Press.
- MACKIE, G. O. (1996). Defensive strategies in planktonic coelenterates. In: *Zooplankton: Sensory Ecology and Physiology* (Lenz, P. H., Hartline, D. K., Purcell, J. E. & Macmillan, D. L., eds), pp. 435–446. Amsterdam: Overseas Publishers Association.
- MCFALL-NGAI, M. J. (1990). Crypsis is the pelagic environment. *Amer. Zool.* **30**, 175–188.
- MEYER, R. A. (1979). Light scattering from biological cells: dependence of backscatter radiation on membrane thickness and refractive index. *Appl. Opt.* **18**, 585–588.
- MIE, G. (1908). Beiträge zur Optik trüber Medien, speziell kolloidalen Metall-lösungen. *Ann Phys.* **25**, 377.
- MOURANT, J. R., FREYER, J. P., HIELSCHER, A. H., EICK, A. A., SHEN, D. & JOHNSON, T. M. (1998). Mechanisms of light scattering from biological cells relevant to noninvasive optical-tissue diagnostics. *Appl. Opt.* **37**, 3586–3593.
- PHILIPSON, B. (1973). Changes in the lens related to the reduction of transparency. *Exp. Eye Res.* **16**, 29–39.
- PRUM, R. O., TORRES, R., WILLIAMSON, S. & DYCK, J. (1999). Two-dimensional Fourier analysis of the spongy medullary keratin of structurally coloured feather barbs. *Proc. R. Soc. Lond. B* **266**, 13–22.
- QUINBY-HUNT, M. S. & HUNT, A. J. (1988). Effects of structure on scattering from marine organisms: Rayleigh-Deybe and Mie predictions. *SPIE Ocean Optics IX* **925**, 288–295.
- TARDIEU, A. & DELAYE, M. (1988). Eye lens proteins and transparency: from light transmission theory to solution x-ray structural analysis. *Ann. Rev. Biophys. Biophys. Chem.* **17**, 47–70.
- THIELE, E. S. (1988). Light scattering by complex microstructures in the resonant regime. Doctoral Dissertation, Materials Science Dept., University of Pennsylvania.
- TROKEL, S. (1962). The physical basis for transparency of the crystalline lens. *Invest. Ophthalmol.* **1**, 493–501.
- VAEZY, S. & CLARK, J. I. (1994). Quantitative analysis of the microstructure of the human cornea and sclera using 2-D Fourier methods. *J. Microscop.* **175**, 93–99.
- VAN DE HULST, H. C. (1957). *Light Scattering by Small Particles*. New York: Dover Publications.
- WILSON, B. C., PATTERSON, M. S., & FLOCK, S. T. (1987). Indirect versus direct techniques for the measurement of the optical properties of tissues. *Photochem. Photobiol.* **46**, 601–608.

APPENDIX*

The following is a proof that the average cross-sectional area of any convex solid is one fourth the total surface area of the solid. First, consider a two-dimensional polygonal object with area, A . Let ϕ be the angle between the object and the beam of light, such that, if $\phi = 0$, the light is perpendicular to the flat surface of the object. Then, the cross-sectional area, A_c , of the object is given by:

$$A_c = A|\cos \phi|.$$

The average cross-sectional area, A_{avg} , is calculated by averaging A_c over all possible orientations. Converting to spherical coordinates and integrating over all solid angles gives,

$$\begin{aligned} A_{avg} &= \frac{1}{4\pi} \int_0^{2\pi} \int_0^\pi A|\cos \phi| \sin \phi \, d\phi \, d\theta \\ &= \frac{1}{4\pi} 4\pi \int_0^{\pi/2} A \cos \phi \sin \phi \, d\phi \\ &= \frac{1}{2} A. \end{aligned}$$

Now, consider an n -sided convex polyhedron with faces that have areas, A^i ($i = 1, \dots, n$). Its cross-sectional area, \mathbf{A}_c , for any orientation, is half the sum of the cross-sectional areas of all the faces, since the sum of the cross-sectional areas of the faces in the shade equals the sum of the cross-sectional areas of the faces in the light, which equals \mathbf{A}_c , i.e.

$$\mathbf{A}_c = \frac{1}{2} \sum_{i=1}^n A^i.$$

The average cross-sectional area, \mathbf{A}_{avg} , of the polyhedron over all orientations is then

$$\begin{aligned} \mathbf{A}_{avg} &= \frac{1}{2} (\sum A^i)_{avg} = \frac{1}{2} \sum A^i_{avg} \\ &= \frac{1}{2} \sum \frac{1}{2} A^i = \frac{1}{2} \frac{1}{2} \sum A^i = \frac{1}{4} \mathbf{S}, \end{aligned}$$

where \mathbf{S} is the total surface area of the polyhedron. Thus, the average projected area is one quarter the total surface area for convex polyhedra. Since any convex solid can be approximated arbitrarily well with convex polyhedra, the result holds for any convex solid.

* The above proof was communicated to the authors by Dr Christopher M. Herald, Department of Mathematics, Swarthmore College, Swarthmore, PA, U.S.A. The authors accept sole responsibility for any errors.